Australas Phys Eng Sci Med (2017) 40:707–716
DOI 10.1007/s13246-017-0554-2

SCIENTIFIC NOTE

Probability density distribution of delta RR intervals: a novel method for the detection of atrial fibrillation

Yanjun Li[1,2] · Xiaoying Tang[1] · Ancong Wang[1] · Hui Tang[3]

Received: 21 August 2015 / Accepted: 1 May 2017 / Published online: 15 June 2017

Abstract Atrial fibrillation (AF) monitoring and diagnosis require automatic AF detection methods. In this paper, a novel image-based AF detection method was proposed. The map was constructed by plotting changes of RR intervals (△RR) into grid panes. First, the map was divided into grid panes with 20 ms fixed resolution in y-axes and 15–60 s step length in x-axes. Next, the blank pane ratio (BPR), the entropy and the probability density distribution were processed using linear support-vector machine (LSVM) to classify AF and non-AF episodes. The performance was evaluated based on four public physiological databases. The Cohen's Kappa coefficients were 0.87, 0.91 and 0.64 at 50 s step length for the long-term AF database, the MIT-BIH AF database and the MIT-BIH arrhythmia database, respectively. Best results were achieved as follows: (1) an accuracy of 93.7%, a sensitivity of 95.1%, a specificity of 92.0% and a positive predictive value (PPV) of 93.5% were obtained for the long-term AF database at 60 s step length. (2) An accuracy of 95.9%, a sensitivity of 95.3%, a specificity of 96.3% and a PPV of 94.1% were obtained for the MIT-BIH AF database at 40 s step length. (3) An accuracy of 90.6%, a sensitivity of 94.5%, a specificity of 90.0% and a PPV of 55.0% were achieved for the MIT-BIH arrhythmia database at 60 s step length. (4) Both accuracy and specificity were 96.0% for the MIT-BIH normal sinus rhythm database at 40 s step length. In conclusion, the intuitive grid map of delta RR intervals offers a new approach to achieving comparable performance with previously published AF detection methods.

Keywords Arrhythmia · Atrial fibrillation (AF) · Grid map · Probability density distribution (PDD) · Delta RR intervals (△RR) · Atrial fibrillation database

Introduction

Atrial arrhythmias are associated with the increased risk of stroke, heart failure and mortality. They consist of atrial escape, premature atrial beat, atrial tachycardia, atrial flutter, and atrial fibrillation (AF), in which AF is the most common sustained atrial arrhythmias and accounts for one-third of the cardiac arrhythmias [1]. Compared with patients without AF, those with AF have a higher risk of stroke or transient ischemic attack [2]. Although the current gold-standard approach to diagnosing AF is 12-lead electrocardiogram (ECG) [3], it is apt to use 3-lead ECG for 24 or 48 h Holter monitoring in both clinical and out-of-clinical settings. Taggar et al. [3] found that automated ECG-interpreting software achieved similar accuracy to that of healthcare professionals, which greatly lightens the burden on general practitioners and nurses within the primary care system.

AF is usually diagnosed by analyzing two groups of features of the ECG: the irregularity of RR intervals (RRI) and the absence of P wave [4]. Some researchers have focused on the features of P waves or f-waves for AF monitoring. P wave-related indices provide a wealth of information in the AF assessment, including PR interval, P wave duration,

✉ Xiaoying Tang
xiaoying@bit.edu.cn

[1] School of Life Science, Beijing Institute of Technology, ZhongGuanCun South Rd 5#, Haidian, Beijing, China

[2] State Key Laboratory of Space Medicine Fundamentals and Application, China Astronaut Research and Training Center, Beijing, China

[3] Hongfeng Control Company of the Sanjiang Space Group, Xiaogan, Hubei, China

P wave terminal force, P wave axis, P wave dispersion and measures of P wave morphology [5]. Petrenas et al. [6] improved AF monitoring with modified Lewis lead and got atrial amplitude three times as large as the original Lewis leads. Increased P wave duration and P wave dispersion reflect prolongation of intra-atrial and inter-atrial conduction time and the inhomogeneous propagation of sinus impulses [7], which are electro-physiologic characteristics in patients with AF during non-AF period. Martinez et al. [8] found that P wave fragmentation and P wave area presented a higher variability 2 h preceding the onset of paroxysmal atrial fibrillation. Asgari et al. [9] achieved a sensitivity of 97.0% and a specificity of 97.1% by using stationary wavelet transform of ECG waveform and support vector machine for the MIT-BIH atrial fibrillation database. Steven et al. [10] proposed a patient specific AF detection method with a Gaussian mixture model of the P wave features, and got a sensitivity of 98.1%, a specificity of 91.7%, and a positive predictive value of 79.2% for the MIT-BIH atrial fibrillation database.

Because TQ intervals are independent of the ventricular activity, several researchers studied the function of TQ intervals for AF detection. Du et al. [11] used the average number of f-waves in TQ intervals as a characteristic parameter for AF detection. The sensitivity, the positive predictive value and the accuracy for multiple combined databases were 94.1, 97.7 and 94.6%, respectively. Rodenas et al. [12] computed the wavelet entropy of TQ intervals on noise-free beats of the ECG to detect the AF episodes. However, both atrial flutter and junctional rhythms were discarded from the ECG before AF detection [12], which is inconsistent with clinical AF identification. Garcia et al. [13] achieved a sensitivity of 91.2% and a specificity of 94.5% for the MIT-BIH atrial fibrillation database with the relative wavelet energy of the TQ intervals.

AF detection based on the P wave or TQ interval is difficult, because the detection of the fiducial point of the P wave is not easy, especially for Holter monitoring applications [14]. Therefore, many studies have used the regularity of RR intervals instead. Nurul et al. [15] found that there is a significant difference between atrial fibrillation patients and healthy humans in features derived from RR intervals (t test, $P < 0.0001$). Oster et al. [16] found a linear decrease in the accuracy of AF detection with respect to the signal quality of RR intervals. Mishra et al. [17] pointed out that removal of abnormal beats will improve the pre-processing of the RR intervals. Marwaha et al. [18] found that AF patients compared with healthy people tend to have a low entropy value of RR intervals. Petrenas et al. [19] proposed an AF detector which involved ectopic beat filtering, bigeminal suppression, and RR interval irregularity calculation, and got a sensitivity of 97.1% and a specificity of 98.3% for the MIT-BIH atrial fibrillation database. Islam et al. [20] achieved a sensitivity of 96.4% and a specificity of 96.4% by estimating the entropy of the distribution of heartbeats for the MIT-BIH atrial fibrillation database. Dash et al. [21] used the turning points ratio, the root mean square of successive RR differences and Shannon entropy to identify AF. They achieved a sensitivity of 94.4% and a specificity of 95.1% for the MIT-BIH atrial fibrillation database, and got a sensitivity of 90.2% and a specificity of 91.2% for the MIT-BIH arrhythmia database [21]. Lee et al. [14] obtained a specificity of 99.7% for the MIT-BIH normal sinus rhythm database, and obtained a sensitivity of 91.1% and a specificity of 89.7% for the MIT-BIH arrhythmia database by time-varying coherence function. Huang et al. [4] used the distribution of the density histogram of delta RR intervals to detect the transition between AF and sinus rhythm, and achieved a sensitivity of 96.1% and a specificity of 98.1% for the MIT-BIH AF database, and a specificity of 97.9% for the MIT-BIH normal sinus rhythm database.

However, most previous studies have limitations due to their computational complexity or unsatisfactory performance. In this paper, a novel method was introduced for the automatic detection of atrial fibrillation. The varying grid map is derived from the difference between successive RR intervals. The variability of RR interval is quantified to detect the AF event by the ratio of blank panes, the entropy and the probability density distribution.

Methods

Database

Four PhysioNet databases, the MIT-BIH atrial fibrillation database, the MIT-BIH arrhythmia database, the long term atrial fibrillation database and the MIT-BIH normal sinus rhythm database [22] were used to verify the performance of the proposed method. All databases above are available freely on the web site "http://www.physionet.org/physiobank/database/", including both ECG data and their corresponding annotation files. Cardiac rhythm information is shown in Table 1, including a total of 175 records with 1379.9 h of normal sinus rhythm, 1126.5 h of AF, and 51.4 h of other rhythms. The atrial flutter (AFL) episodes were treated as non-AF [4]. The annotation of RR intervals and cardiac rhythm in the database were used directly. Thus, for each record, a list of labeled RR intervals was obtained for further processing, and their corresponding annotations of AF and non-AF rhythm were used as the references for the performance evaluation.

Table 1 Statistics of the databases

Database	MIT-BIH AF database	MIT-BIH arrhythmia database	Long term AF database	MIT-BIH normal sinus rhythm database	Combined databases
Sampling rates (Hz)	250	360	128	128	–
A/D bits	12	11	12	12	–
Number of all records	25	48	84	18	175
Number of records with AF	25	8	83	0	116
Total time (h)	249.2	24.1	1900.3	384.2	2557.8
Time of normal sinus rhythm (h)	149.1	18.1	828.5	384.2	1379.9
AF total time (h)	93.5	2.1	1030.9	0	1126.5
Other rhythms (h)	6.6	3.9	40.9	0	51.4
Percent of normal sinus rhythm (%)	59.8	75.1	43.6	100	54.0
Percent of AF (%)	37.5	8.7	54.3	0	44.0
Percent of other rhythms (%)	2.7	16.2	2.2	0	2.0

Methods

The proposed method contains three main steps: (1) construction of the varying grid map using the difference of RR intervals ($\triangle$RR); (2) construction of the probability density distribution (PDD) from the varying grid map; (3) AF event detection using linear support-vector machine (LSVM) with input vectors that consist of the blank pane ratio (BPR), the entropy and the PDD. Finally, results were compared with the annotation from four open databases.

The $\triangle$RR is defined as the difference between two successive RR intervals, and the varying grid map is defined as the distribution of the $\triangle$RR that mapped into the grid panes. Figure 1 illustrates the procedures of the proposed method. An example of this method is illustrated in Fig. 2.

Construction of varying grid map

The fluctuation of RR interval reveals the variation of the cardiac rhythm. It is the most important characteristic used to distinguish AF rhythm from others, because RR interval varies irregularly during the AF rhythm. The original $\triangle$RR derived from the RR intervals is defined as $\triangle RR_1$.

Firstly, $\triangle RR_2$ is derived from $\triangle RR_1$ by formula (1). For example, data in Fig. 2b that exceed TH_1 are reset as TH_1 while data that exceed $-TH_1$ are reset as $-TH_1$ in Fig. 2c.

$$\Delta RR_2(n) = \begin{cases} \Delta RR_1(n), & where\ |\Delta RR_1(n)| \le TH_1 \\ TH_1, & where\ \Delta RR_1(n) > TH_1 \\ -TH_1, & where\ \Delta RR_1(n) < -TH_1 \end{cases} \quad (1)$$

where n is the serial number of the discrete sequence $\{\triangle RR_1(n)\}$ and $\{\triangle RR_2(n)\}$.The threshold TH_1 is fixed as 400 ms in this paper.

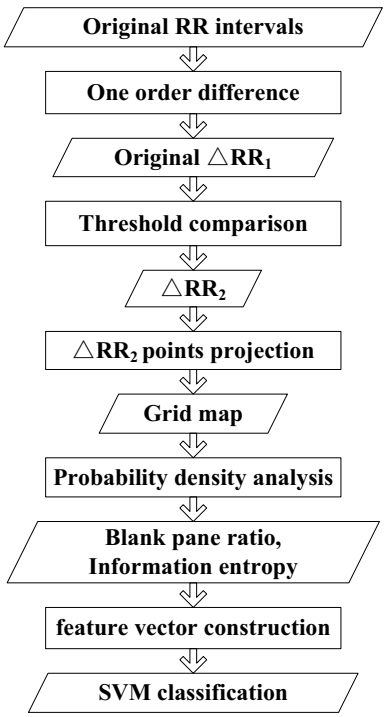

Fig. 1 Procedure of the proposed method

Secondly, the grid map is constructed by using the $\triangle RR_2$. Using the point (0, 0) as the reference point in the rectangular coordinates, the distribution of $\triangle RR_2$ is divided up into small rectangle panes, while the size of the panes is fixed at the height and the width. For example, the height is 20 ms and the width is 30 s for every pane in Fig. 2c, indicating that the grid resolution was fixed at 20 ms in y-axes and 30 s in x-axes.

Figure 2 is one example that most segments of the last half part are AF segments. The irregular inter-beat intervals during AF episodes in Fig. 2a leads to the irregular

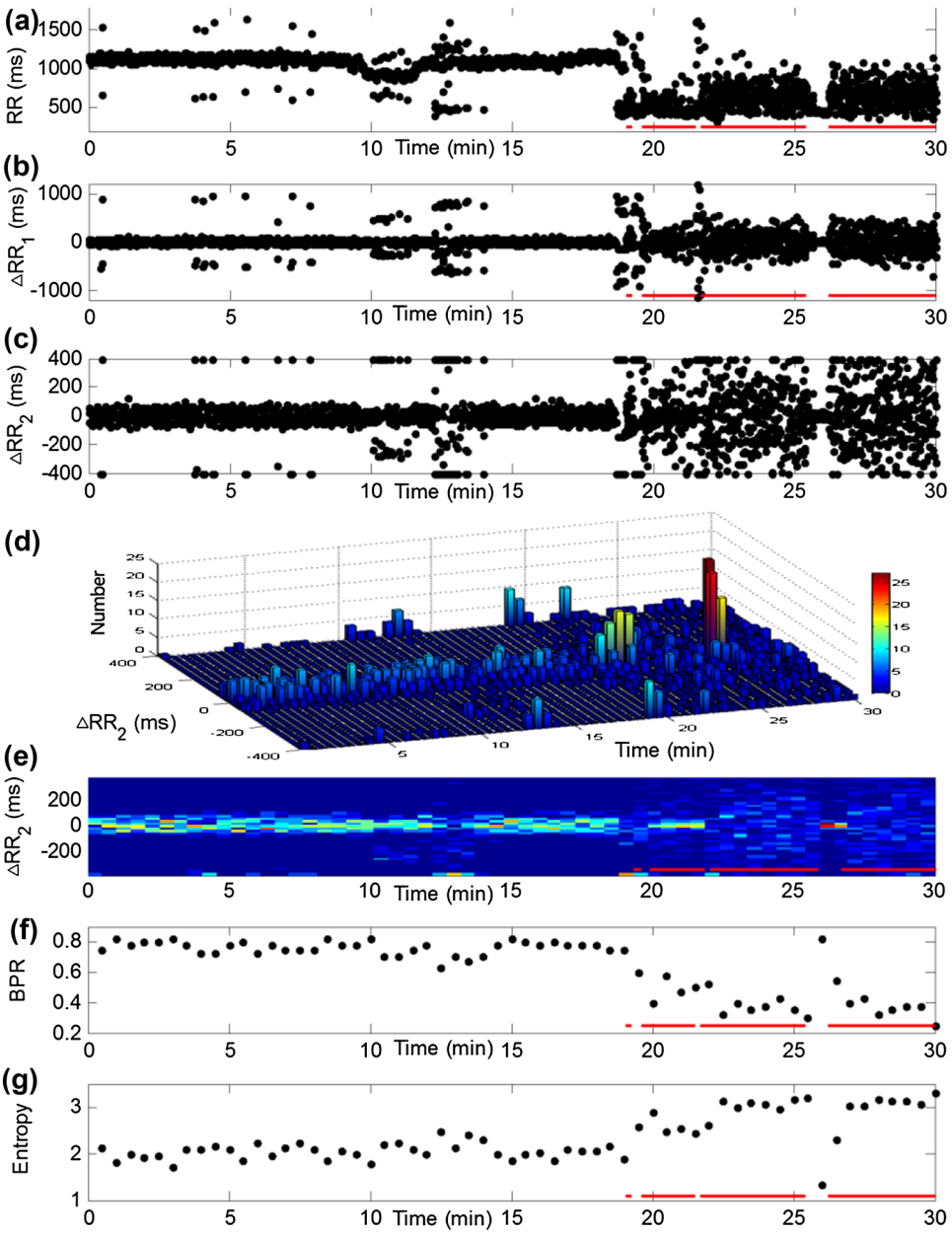

Fig. 2 Construction of probability density distribution of record '202' of the MIT-BIH arrhythmia database. **a** RR interval; **b** $\triangle RR_1$, derived from RR interval; **c** $\triangle RR_2$, derived from $\triangle RR_1$, the grid resolution is fixed at 20 ms in y-axes and at 30 s in x-axes; **d** number of $\triangle RR_2$ points in each pane; **e** probability density distribution of $\triangle RR_2$; **f** blank pane ratio, derived from the varying grid map; **g** entropy, derived from the varying grid map. The *solid lines* at the *bottom* of **a, b, e–g** are the annotation of AF event in the database

distribution of $\triangle RR_1$ in Fig. 2b. In Fig. 2b, the point around the zero level indicates that the former RR interval and the latter RR interval are almost the same. In Fig. 2c, AF rhythm is characterized by the scattered $\triangle RR_2$ points that are distributed in a large area, reflecting the irregularity of the changes of heart rate. In contrast, $\triangle RR_2$ data of non-AF rhythm are usually distributed in a small area, implying the presence of rhythm regularity. The number of $\triangle RR_2$ points in every pane is shown in Fig. 2d. In Fig. 2e, AF is represented in the form of diffusion panes with low probability density, while non-AF is associated with sparse panes with focused and high probability density. As shown in Fig. 2f, the AF segments are associated with low density empty panes, while non-AF segments are associated with high density empty panes. As shown in Fig. 2g, the AF segments are associated with high entropy, while non-AF segments are associated with low entropy. The red solid lines at the bottom of Fig. 2a, b, e–g correspond to the AF event annotations in the database.

Construction of probability density distribution map

The PDD map in Fig. 2e is defined by the following steps.

1. Construction of matrix X with the number of points that are projected into the panes. In formula (2), $s_{i,j}$ represents the number of $\triangle RR_2$ points which projected into the (i, j) pane of matrix $\boldsymbol{X}$.

$$X = \begin{bmatrix} s_{1,1} & s_{1,2} & \cdots & s_{1,N} \\ s_{2,1} & s_{2,2} & \cdots & s_{2,N} \\ \vdots & \vdots & \cdots & \vdots \\ s_{M,1} & s_{M,2} & \cdots & s_{M,N} \end{bmatrix} \quad (2)$$

Define the height of every pane as s_y in y-axes and the width as s_x in x-axes, while M and N in formula (2) is calculated by formula (3) and formula (4), respectively. During the AF detection, s_x and s_y were set to the same scale to measure the irregularity of heartbeats for both AF and non-AF rhythms.

$$M = 2 \times TH_1 / s_y \quad (3)$$

$$N = t / s_x \quad (4)$$

where t is the total length of RR intervals.

An example is shown in Fig. 2d, where t = 1800s, TH_1 = 400 ms, s_y = 20 ms and s_x = 30 s. Therefore, M = 2 × 400/20 = 40, N = 1800/30 = 60. Thus, totally there are 40 × 60 = 2400 panes in Fig. 2d.

2. Construction of PDD map (matrix ***P***). Each element in matrix ***P*** is calculated by formula (6). If the (i, j) pane is empty, then both $s_{i,j}$ and $p_{i,j}$ are equal to zero. The empty rectangle panes are shown with the color of deep blue in Fig. 2d, e.

$$P = \begin{bmatrix} p_{1,1} & p_{1,2} & \cdots & p_{1,N} \\ p_{2,1} & p_{2,2} & \cdots & p_{2,N} \\ \vdots & \vdots & \cdots & \vdots \\ p_{M,1} & p_{M,2} & \cdots & p_{M,N} \end{bmatrix} \quad (5)$$

$$p_{i,j} = \frac{s_{i,j}}{\sum_{k=1}^{M} s_{k,j}} \quad (6)$$

3. Calculation of the BPR. One blank pane is a pane without any ΔRR_2 projected into it. BPR is defined as the ratio of the number of blank panes to the number of all panes in each column of matrix ***X***. For instance, suppose there are 40 panes in one column of matrix ***X*** and the number of blank panes in this column is 30, then BPR = 30/40 = 0.75.
4. Calculation of the entropy. The information entropy (Shannon entropy) is calculated by formula (7). As shown in Fig. 2g, AF is indicated by higher entropy than non-AF, meaning AF in Fig. 2e is accompanied by higher uncertainty and unpredictability.

$$I_j = -\sum_{k=1}^{M} p_{k,j} \times \log(p_{k,j}) \quad (7)$$

AF detection using the LSVM

An AF event is found using the LSVM with input vectors of ΔRR_2.

1. Construct the feature vectors for LSVM. The input feature vector v_j for LSVM is constructed with the BPR, the entropy and the PDD as follows,

$$v_j = \left[BPR_j \; I_j \; p_{1,j} p_{2,j} p_{3,j} \cdots p_{M,j} \right] \quad (8)$$

where j is the jth episode, while each episode duration could be 15, 20, 30, 40, 50 or 60 s. As M = 40, there are 42 elements in each feature vector.

2. AF detection with LSVM. In this paper, LSVM classifier was implemented using LIBSVM toolbox, which is available at "http://www.csie.ntu.edu.tw/~cjlin/libsvm/". Leave-one-record-out strategy is used for training LSVM. For each test record, the corresponding LSVM was trained with the remaining 174 records from the combined database. The successive AF segments are combined as one AF episode, and all heartbeats within the AF episode are considered as AF heartbeats, while all heartbeats outside the AF episode are considered as non-AF heartbeats.

Validation and performance assessment

The performance was tested on four PhysioNet databases, including the MIT-BIH atrial fibrillation database, the MIT-BIH arrhythmia database, the long term AF database, and the MIT-BIH normal sinus rhythm database [22]. The accuracy (ACC), the sensitivity (SEN), the specificity (SPE) and the positive predictive value (PPV) were calculated for each database according to the formulas (9–12), respectively. If there are AF heartbeats in one episode, this episode is considered as AF episode, otherwise it is considered as non-AF episode.

$$ACC = (TP + TN)/(TP + TN + FP + FN) \quad (9)$$

$$SEN = TP/(TP + FN) \quad (10)$$

$$SPE = TN/(TN + FP) \quad (11)$$

$$PPV = TP/(TP + FP) \quad (12)$$

where TP is the number of AF episodes that are annotated in the database which are classified as AF episodes by the classifier. TN is the number of non-AF episodes that are annotated in the database which are classified as non-AF episodes by the classifier. FP is the number of non-AF

episodes that are annotated in the database which are classified as AF episodes by the classifier. FN is the number of AF episodes that are annotated in the database which are classified as non-AF episodes by the classifier.

Moreover, the Cohen's Kappa is used to assess the episode-by-episode agreement between the reference episodes and the detection results. When Kappa is higher than 0.75, it is good; while when it is smaller than 0.40, it is poor; otherwise it is fair.

According to Table 1, there are no AF episodes in the MIT-BIH normal sinus rhythm database, indicating that TP = 0 and FN = 0. Thus, formula (9) is equal to formula (11) in such condition, making ACC equal to SPE. Moreover, both sensitivity and PPV are not accessible according to formula (10) and formula (12) when TP = 0 and FN = 0.

Results

AF detection results from each database

The performance of the method was evaluated using four public physiological databases. As it is shown in Fig. 3, the map is divided into grid panes with a fixed 20 ms resolution in y-axes and 15–60 s step length in x-axes. The method maintains high accuracy even for 15 s-data segments. Comparing the different step length in x-axes, the best results were obtained as follows: (1) an accuracy of 93.7%, a sensitivity of 95.1%, a specificity of 92.0% and a PPV of 93.5% were obtained for the long-term AF database at 60 s step length. (2) An accuracy of 95.9%, a sensitivity of 95.3%, a specificity of 96.3% and a PPV of 94.1% were obtained for the MIT-BIH AF database with 40 s step length. (3) An accuracy of 90.6%, a sensitivity of 94.5%, a specificity of 90.0% and a PPV of 55.0% were achieved for the MIT-BIH arrhythmia database at 60 s step length. (4) Both accuracy and specificity were 96.0% for the MIT-BIH normal sinus rhythm database at 40 s step length, because the accuracy is equal to the specificity according to formulas (8) and (10) when TP = 0 and FN = 0. Besides, both PPV and sensitivity are not accessible for the MIT-BIH normal sinus rhythm database.

Furthermore, the Cohen's Kappa coefficients were 0.87, 0.91 and 0.64 at 50 s step length for the long-term AF database, the MIT-BIH AF database and the MIT-BIH arrhythmia database, respectively. However, Cohen's Kappa coefficient is not accessible for the MIT-BIH normal sinus rhythm database because it has only normal rhythm.

Figure 4 shows the results of AF detection for four records '00', '28', '72' and '115' in the long term AF

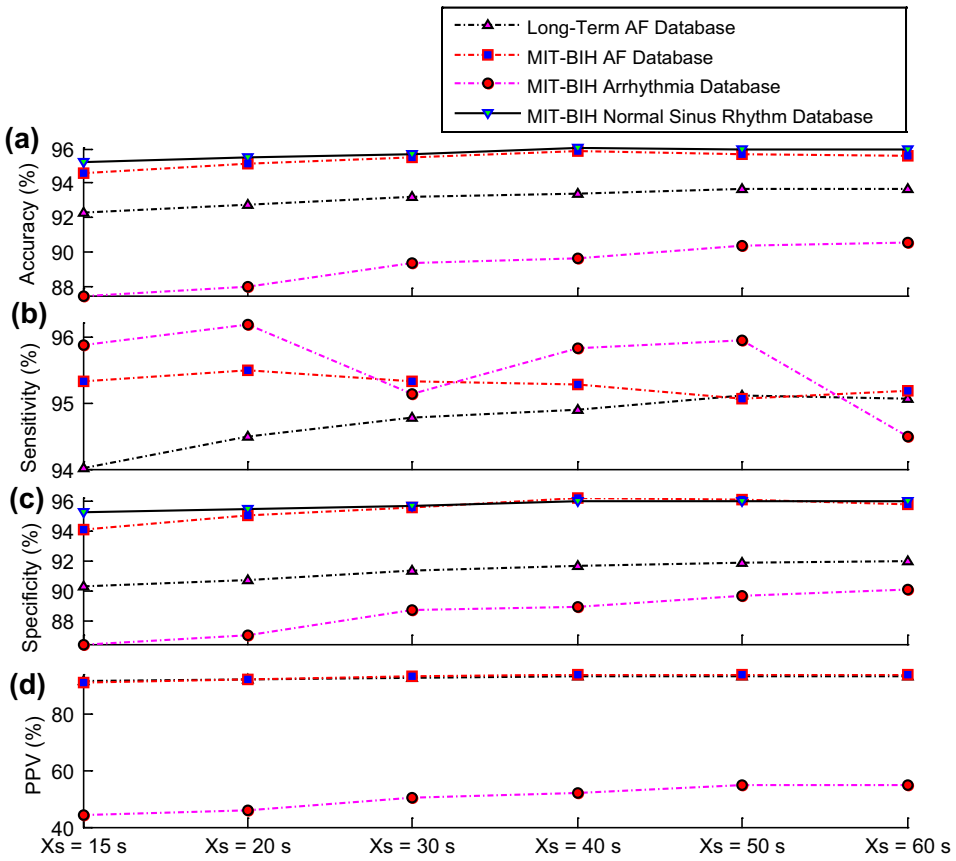

Fig. 3 AF detection results for each database

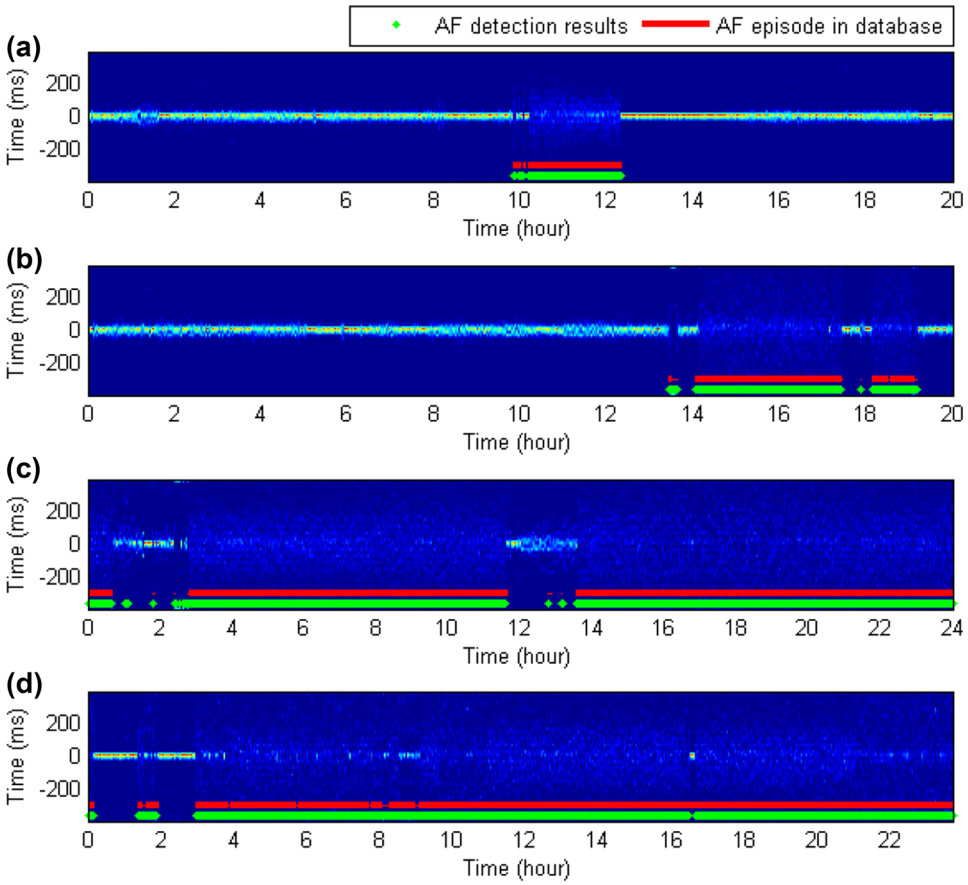

Fig. 4 Results of AF detection for four records in the long term AF database. **a** Record '00', **b** record '28', **c** record '72' and **d** record '115'. The *red solid line* at the *bottom* is the annotation of AF event in the database, and the *green points* are the detected AF results

database. The accuracy was 98.8, 99.2, 99.2 and 93.4%, respectively, and Cohen's Kappa coefficients were 0.94, 0.98, 0.97 and 0.73, respectively.

Comparison with published algorithms

A comparison with some published algorithms for the public databases is listed in Table 2. The sensitivity and the specificity are mostly used by their meaningful clinical measurements of true-positive rate and true-negative rate. However, the PPV is affected by the prevalence of AF arrhythmia.

The performance of this proposed algorithm was comparable to most of the published algorithms. The accuracy of this proposed algorithm is 95.9% for the MIT-BIH AF database, while the best accuracy is 97.9% [14]. The accuracy of this proposed algorithm is 96.0% for the MIT-BIH normal sinus rhythm database, while the best accuracy is 99.7% [14]. The accuracy of this proposed algorithm is 90.6% for the MIT-BIH arrhythmia database, which was comparable to the best accuracy of 91.5% [28]. The accuracy of the proposed method is 93.7% for the long-term AF database, which is comparable to the best accuracy of 96.1% [28]. It indicates that the methods from [14, 28] accomplished the highest accuracies. Furthermore, both of them are RRI-based method, which proved that RRI-based methods usually show higher performance than methods based on P waves. Moreover, most methods in Table 2 are RRI-based and only two methods are P wave-based, which partially proves that RRI-based algorithms are easier to be implemented than P wave-based algorithms.

The accuracy is 90.6% for the MIT-BIH arrhythmia database, which is much lower than the other three databases. Even worse, the PPV is only 55.0%, which means only half of the detected AF episodes are real AF episodes, but the other half are non-AF episodes. According to Table 1, the proportion of non-AF arrhythmias is 16.2% in the MIT-BIH arrhythmia database, while in any other database it is lower than 3%. Irregularity of heart rates is not only the feature of AF rhythm, but also the feature in some non-AF arrhythmias (such as atrial flutter). For example, one event of irregular RR intervals with 291 s duration in the record 203 of the MIT-BIH arrhythmia database is AFL rather than AF, however the proposed algorithm mistook this AFL event as AF event. Therefore, methods using only RR intervals tend to confuse AF with other non-AF arrhythmias. As the MIT-BIH arrhythmia database contains various forms of ectopic beats and many non-AF arrhythmias, the performance was worse for the MIT-BIH arrhythmia database than for other three databases.

Table 2 Comparison of recent published algorithms

Database	Methods	ACC (%)	SEN (%)	SPE (%)	PPV (%)
MIT-BIH AF database	Lian et al. [23][a]	NP	94.3	95.1	NP
	Dash et al. [21][a]	NP	94.4	95.1	NP
	Tateno et al. [24][a]	NP	94.4	97.2	NP
	Logan et al. [25][a]	NP	96.0	89.0	NP
	Kikillus et al. [26][a]	NP	94.4	93.4	NP
	Lake et al. [27][a]	NP	91.0	94.0	NP
	García et al. [13][a]	93.3	91.2	94.5	NP
	Islam et al. [20][a]	96.4	96.4	96.4	NP
	Ladavich et al. [10][b]	NP	98.1	91.7	79.2
	Zhou et al. [28][a]	97.7	96.9	98.3	97.6
	Rodenas et al. [12][a]	95.3	96.5	94.2	NP
	Lee et al. [14][a]	97.9	98.2	97.7	96.9
	Huang et al. [4][a]	NP	96.1	98.1	NP
	Asgari et al. [9][b]	NP	97.0	97.1	NP
	Petrėnas et al. [19][a]	NP	97.1	98.3	NP
	Our way[a]	95.9	95.3	96.3	92.0
MIT-BIH normal sinus rhythm database	Lian et al. [23][a]	84.1	NA	84.1	NA
	Kikillus et al. [26][a]	96.9	NA	96.9	NA
	Huang et al. [4][a]	97.9	NA	97.9	NA
	Zhou et al. [28][a]	98.3	NA	98.3	NA
	Lee et al. [14][a]	99.7	NA	99.7	NA
	Our way[a]	96.0	NA	96.0	NA
MIT-BIH arrhythmia database	Lee et al. [14][a]	NP	91.1	89.7	NP
	Lian et al. [23][a]	NP	98.1	77.0	NP
	Dash et al. [21][a]	NP	90.2	91.2	NP
	Garcia et al. [13][a]	90.8	91.1	90.4	NP
	Zhou et al. [28][a]	91.5	97.3	90.8	55.3
	Our way[a]	90.6	94.5	90.0	55.0
Long-term AF database	Zhou et al. [28][a]	96.1	96.7	95.1	96.6
	Our way[a]	93.7	95.1	92.0	93.5

NP not provided by the authors, *NA* not accessible

[a]RRI-based algorithm

[b]P wave-based algorithm

Discussion

AF detection based on the irregularity of RR intervals

ECG-based AF detection relies either on the absence of P waves or on the irregularity of RR variability. P wave-related algorithms are targeted in the atrial activity, which provide a lot of information on AF estimation, but P wave indices are usually associated with low SNR. The low amplitude of the P wave in the ECG is usually influenced by various noises, therefore it is difficult to locate the fiducial point of the P wave. RRI-based algorithms are targeted at only measuring the rhythm of ventricular activity, making most use of the dynamics of RR intervals and only require the identification of the R-wave. RRI is associated with high SNR, but is focused on the ventricular activity rather than the atrial activity.

Different heart rhythms show distinctive spatial distribution patterns in their $\triangle$RR maps. In particular, AF rhythm is characterized with random data points scattered in a large area on the $\triangle$RR map, which reflect the irregularity of RR intervals [23]. To quantify the sparseness of data points, in this paper the $\triangle$RR map was divided by a 2-dimensional grid with fixed resolution in the horizontal axes and vertical axes. The ratio of empty panes, the entropy and the probability density feature were counted to distinguish AF rhythm from non-AF rhythm. The feature of AF episode is depicted based on the distribution of $\triangle$RR in the varying grid map along with time, so that the automated algorithm does not require any human intervention. The AF episodes

are characterized by the low value of BPR, high entropy and high density of non-empty panes, while the non-AF episodes correspond to the high value of BPR, low entropy and low density of non-empty panes. The performance of the new AF detection algorithm was evaluated using 4 annotated PhysioNet databases. Our method achieved comparable performance with most of the existing methods.

Construction of the map of delta RR intervals

The structure of ΔRR map is different from that of Poincare plots. In the Poincare plots, both x-axis and y-axis are inter-beat intervals. However, in the ΔRR map, the y-axis is the difference of successive inter-beat intervals while the x-axis is a time span. The Poincare plots show the statistical distribution of RR intervals during certain period of time, while the varying grid map of delta RR intervals presents the dynamic distribution of ΔRR in time axes. Lian et al. [23] also used a grid map to quantify the distribution of RR intervals and the corresponding ΔRR, using RR intervals as the x-coordinates while ΔRR as the y-coordinates. However, such grid maps could not show the dynamic distribution of RR intervals along with time span. As shown in Fig. 4, our grid map could easily show the dynamic distribution of ΔRR during 24 h' time. Conversely, it needs many maps to reveal the feature of several hours' data with the way of Poincare plots. Moreover, our algorithm outperformed that of Lian et al. [23] for both the MIT-BIH normal sinus rhythm database and the MIT-BIH AF database, as shown in Table 2.

The average value of ΔRR is close to zero, while the average value of RR intervals is different from person to person and from moment to moment. Therefore, delta RR intervals are more proper than RR intervals for the construction of varying grid map, making the middle line of the map close to zero. However, even for ΔRR map, sometimes there are a few data exceeding certain threshold. If the range of ΔRR map is set as the maximum and the minimum of ΔRR, the BPR will always be very high because there are many blank panes, no matter whether AF happens or not. Consequently, the data exceeding certain threshold were reset as the threshold in this paper, making the BPR quite different for AF events and non-AF events.

Limitation

There are several limitations in our study. Firstly, we do not propose an effective method for detecting very short AF episodes, e.g., the setting of 15 s window width may cause the short AF episodes whose duration is <15 s to evade detection. In our study, the best window width was 60 s for the MIT-BIH arrhythmia database. For instance, the shortest AF episode in record 203 of the MIT-BIH arrhythmia database is only 0.6 s (only one heartbeat), happening at 5 min:04 s from the beginning of the recording, immediately followed by a ventricular tachycardia episode. Such short AF episodes were missed in our AF detection process.

Secondly, like all other RR intervals-based algorithms, the present method may fail to detect AF with relatively regular rhythm and may produce a false alarm for non-AF rhythm with a certain degree of rhythm irregularity, or may mistake the atrial flutter episodes in an irregular rhythm for AF episodes.

These two limitations above are easy to be overcome by P wave-based AF detection methods [10], but P wave-based methods are suffering from low positive predictive value, e.g., the PPV in only 79.2% for the MIT-BIH atrial fibrillation database with a Gaussian mixture model of the P wave features, while RRI-based method can obtain a PPV of 97.6% [28].

Perspectives

RRI-based method cannot find AF episodes if only a few heartbeats are available for analysis. Even worse, it often fails to detect AF in a regular rhythm or mistakes the atrial flutter episodes in an irregular rhythm for AF episodes. On the other hand, P wave-based methods are suffering from low SNR of P waves. Therefore, the combination of P wave (or f-wave) with RR intervals will facilitate the discrimination of various cardiac arrhythmias and yields a better AF detector. Moreover, clinical practice needs to evaluate the effects of artifacts on RR intervals for AF detection.

Conclusion

A novel image-based method for detecting atrial fibrillation was developed and evaluated using RR intervals in this paper. The new AF detection algorithm utilizes a map that plots changes of RR intervals (ΔRR) versus time. The map is divided by a grid with fixed resolution in x-axes and y-axes. The ratio of empty panes, the entropy and the probability density distribution of ΔRR are combined to classify AF and non-AF episodes. The method achieved comparable performance in comparison with published AF detection methods.

In conclusion, the blank pane ratio, the entropy and the probability density distribution of ΔRR map are novel indices to reveal the important characteristic of irregularity of RR intervals during an AF event, and the intuitive grid map of delta RR intervals offers a new approach to AF detection.

Acknowledgements This study was funded by State Key Laboratory of Space Medicine Fundamentals and Application, China Astronaut Research and Training Center (SMFA15B06, SMFA15A01), and it was also funded by China National Natural Science Fund (81471743, 81601561, 61401417).

Compliance with ethical standards

Conflict of interest The authors declare that there is no conflict of interest regarding the publication of this article.

Ethical approval This article does not contain any studies with human or animal subjects performed by any of the authors.

Informed consent All data used in this paper are from the open databases of the PhysioNet "http://www.physionet.org/physiobank/database/".

References

1. Rieta JJ, Ravelli F, Sornmo L (2013) Advances in modeling and characterization of atrial arrhythmias. Biomed Signal Process 8(6):956–957
2. Sposato LA, Cipriano LE, Saposnik G et al (2015) Diagnosis of atrial fibrillation after stroke and transient ischaemic attack: a systematic review and meta-analysis. Lancet Neurol 14(4):377–387
3. Taggar JS, Coleman T, Lewis S et al (2015) Accuracy of methods for diagnosing atrial fibrillation using 12-lead ECG: a systematic review and meta-analysis. Int J Cardiol 184:175–183
4. Huang C, Ye S, Chen H et al (2011) A novel method for detection of the transition between atrial fibrillation and sinus rhythm. IEEE Trans Bio Med Eng 58(4):1113–1119
5. German DM, Kabir MM, Dewland TA et al (2016) Atrial fibrillation predictors: importance of the electrocardiogram. Ann Noninvasive Electrocardiol 21(1):20–29
6. Petrenas A, Marozas V, Jarusevicius G et al (2015) A modified Lewis ECG lead system for ambulatory monitoring of atrial arrhythmias. J Electrocardiol 48:157–163
7. Okutucu S, Aytemir K, Oto A (2016) P-wave dispersion: what we know till now? JRSM Cardiovasc Dis 5:1–9
8. Martinez A, Alcaraz R, Rieta JJ (2014) Morphological variability of the P-wave for premature envision of paroxysmal atrial fibrillation events. Physiol Measurement 35:1–14
9. Asgari S, Mehrni A, Moussavi M (2015) Automatic detection of atrial fibrillation using stationary wavelet transform and support vector machine. Comput Biol Med 60:132–142
10. Ladavich S, Ghoraani B (2015) Rate-independent detection of atrial fibrillation by statistical modeling of atrial activity. Biomed Signal Process Control 8:274–281
11. Du X, Rao N, Qian M et al (2014) A novel method for real-time atrial fibrillation detection in electrocardiograms using multiple parameters. Ann Noninvasive Electrocardiol 19(3):217–225
12. Rodenas J, García M, Alcaraz R et al (2015) Wavelet entropy automatically detects episodes of atrial fibrillation from single-lead electrocardiograms. Entropy 17:6179–6199
13. Garcia M, Rodenas J, Alcaraz R et al (2016) Application of the relative wavelet energy to heart rate independent detection of atrial fibrillation. Comput Methods Progr Biomed 131:157–168
14. Lee J, Nam Y, McManus DD et al (2013) Time-varying coherence function for atrial fibrillation detection. IEEE Trans Bio Med Eng 60(10):2783–2793
15. Nurul AA, Norlaili MS, Mohd AO (2016) Atrial fibrillation classification and association between the natural frequency and the autonomic nervous system. Int J Cardiol 222:504–508
16. Oster J, Clifford GD (2015) Impact of the presence of noise on RR interval-based atrial fibrillation detection. J Electrocardiol 48:947–951
17. Mishra A, Swati D (2015) The recursive combination filter approach of pre-processing for the estimation of standard deviation of RR series. Australas Phys Eng Sci Med 38:413–423
18. Marwaha P, Sunkaria RK (2016) Complexity quantification of cardiac variability time series using improved sample entropy (I-SampEn). Australas Phys Eng Sci Med. doi:10.1007/s13246-016-0457-7
19. Petrenas A, Marozas V, Sornmo L (2015) Low-complexity detection of atrial fibrillation in continuous long-term monitoring. Comput Biol Med 65:184–191
20. Islam MS, Ammour N, Alajlan N et al (2016) Rhythm-based heartbeat duration normalization for atrial fibrillation detection. Comput Biol Med 72:160–169
21. Dash S, Chon KH, Lu S et al (2009) Automatic real time detection of atrial fibrillation. Ann Biomed Eng 37(9):1701–1709
22. Goldberger AL, Amaral LAN, Glass L et al (2000) PhysioBank, PhysioToolkit, and PhysioNet: components of a new research resource for complex physiologic signals. Circulation 101(23):e215–e220. http://www.physionet.org/physiobank/database/
23. Lian J, Wang L, Muessig D (2011) A simple method to detect atrial fibrillation using RR intervals. AM J Cardiol 107(10):1494–1497
24. Tateno K, Glass L (2001) Automatic detection of atrial fibrillation using the coefficient of variation and density histograms of RR and delta RR intervals. Med Biol Eng Comput 39(6):664–671
25. Logan B, Healey J (2005) Robust detection of atrial fibrillation for a long term telemonitoring system. Comput Cardiol 32(1):619–622
26. Kikillus N, Hammer G, Lentz N et al (2007) Three different algorithms for identifying patients suffering from atrial fibrillation during atrial fibrillation free phases of the ECG. Comput Cardiol 34(1):801–804
27. Lake DE, Moorman JR (2011) Accurate estimation of entropy in very short physiological time series: the problem of atrial fibrillation detection in implanted ventricular devices. AM J Physiol Heart C 300(1):319–325
28. Zhou X, Ding H, Ben J (2014) Automatic online detection of atrial fibrillation based on symbolic dynamics and Shannon entropy. BioMed Eng Online 13:18. http://www.biomedical-engineering-online.com/content/13/1/18